HHS Public Access

Author manuscript

J Pharmacokinet Pharmacodyn. Author manuscript; available in PMC 2021 December 01.

Published in final edited form as:

J Pharmacokinet Pharmacodyn. 2020 December ; 47(6): 597–612. doi:10.1007/s10928-020-09713-0.

Development of a Physiologically-Based Pharmacokinetic Model for Ocular Disposition of Monoclonal Antibodies in Rabbits

David Bussing, **Dhaval K Shah***

Department of Pharmaceutical Sciences, School of Pharmacy and Pharmaceutical Sciences, The State University of New York at Buffalo, 455 Pharmacy Building, Buffalo, New York, 14214-8033, USA

Abstract

Development of protein therapeutics for ocular disorders, particularly age-related macular degeneration (AMD), is a highly competitive and expanding therapeutic area. However, the application of a predictive and translatable ocular PK model to better understand ocular disposition of protein therapeutics, such as a physiologically-based pharmacokinetic (PBPK) model, is missing from the literature. Here, we present an expansion of an antibody platform PBPK model towards rabbit and incorporate a novel anatomical and physiologically relevant ocular component. Parameters describing all tissues, flows, and binding events were obtained from existing literature and fixed *a priori*. First, translation of the platform PBPK model to rabbit was confirmed by evaluating the model's ability to predict plasma PK of a systemically administered exogenous antibody. Then, the PBPK model with the new ocular component was validated by estimation of serum and ocular (i.e. aqueous humor, retina, and vitreous humor) PK of two intravitreally administered monoclonal antibodies. We show that the proposed PBPK model is capable of accurately (i.e. within 2-fold) predicting ocular exposure of antibody-based drugs. The proposed PBPK model can be used for preclinical-to-clinical translation of antibodies developed for ocular disorders, and assessment of ocular toxicity for systemically administered antibody-based therapeutics.

Keywords

Eye; Ocular Pharmacokinetics; Antibody; Rabbit; Physiologically-Based Pharmacokinetic Model

Introduction

Diseases of the eye have significant impacts on the lives of patients ranging from transient irritation to irreversible vision loss. Of the ocular disorders, age-related macular degeneration (AMD) and diabetic retinopathy (DR) are among the leading causes of

***Corresponding Author** Dhaval K. Shah, PhD, Telephone: 716-645-4819, dshah4@buffalo.edu.

blindness and are primary indications for protein therapeutics[1,2]. In fact, all four FDA-approved therapies for AMD and DR are macromolecules: Macugen (pegaptanib, Gilead Sciences, Inc), Lucentis (ranibizumab, Genentech, Inc), Eylea (aflibercept, Regeneron Pharmaceuticals, Inc.), and Beovu (brolucizumab, Novartis International AG). With AMD alone expected to reach a global market of $10.4 billion by 2024, research in eye disease remains active and will benefit greatly from new tools that accelerate protein therapeutic drug development[3]. One such tool is pharmacokinetic (PK) models, which can help in characterization and *a priori* prediction of the ocular PK of protein therapeutics.

Existing ocular PK models for protein therapeutics take empiric or traditional compartmental approaches, although recent efforts incorporate more mechanistic aspects, such as tissue permeability and fixed anatomical volumes[4-7]. Currently, there are no mathematical models that characterize PK of protein therapeutics in the eye using purely physiologic parameters. Moreover, as most preclinical studies (e.g. in rabbits) collect only vitreous humor (VH), aqueous humor (AH), and occasionally retina for analysis, the PK in the rest of the ocular tissues is neglected. A physiologically-based pharmacokinetic (PBPK) model for the eye will help in accurately predicting the PK of a drug in all ocular tissues, including the retina and the frequently overlooked cornea, iris-ciliary body (ICB), and choroid. Thus, modelling the exposure in all the tissues of the eye will aid in the development of protein therapeutics for numerous ocular disorders, not just retinopathies.

Predicting the ocular exposure of protein therapeutics with the PBPK model can also help in evaluating the potential of drug induced toxicities in the eye. Antibodies for chemotherapy are targeted agents that are meant to be efficacious against cancerous cells that overexpress a specific antigen. However, presence of the target in healthy tissue, even at low levels, carries the risk of off-target, ocular toxicities, such as corneal microcysts, keratitis, and blurred vision [8-11], Several antibodies against various anti-cancer antigens currently used in therapy have shown potential ocular toxicities including Herceptin (trastuzumab, Genentech, Inc), Kadcyla (trastuzumab emtansine, Genentech, Inc.), Yervoy (ipilimumab, Bristol-Myers Squibb), and Erbitux (cetuximab, Eli Lilly). Ideally, the ocular PBPK model predicts concentrations in the eye tissues based on systemic exposure and can provide a risk assessment for ocular toxicity potential.

Since the 1980s, pharmacometricians have had great interest in the development of PBPK models for protein therapeutics[12-16]. In addition to predicting concentrations at the tissue level, PBPK models also take into account complex interactions between the drug and the proteins in the body, such as FcRn and antigen targets. With a PBPK model, the plasma and tissue-specific PK of a therapeutic can be predicted based on drug-specific parameters that can be obtained in vitro. Furthermore, PBPK models are easily translated between species. Characterization of a drug's PK in one species can be used to predict the PK in another species, simply by changing the physiological parameters of the system.

In 2012, Shah and Betts[16], proposed a platform PBPK model to characterize the plasma and tissue PK of several monoclonal antibodies in mice, rats, monkeys, and human. In this manuscript we have presented the expansion of this platform PBPK model to include rabbit as an additional species. Specifically, rabbits were chosen as they are a predominant species

used in ocular research[17,18] and in antivenom research[19-22], both fields that focus on the development of immunoglobulin (IgG)-based therapies.

In particular, the capabilities of PBPK modelling are currently underutilized in ocular research. Thus, our goal is to expand the platform PBPK model for antibody disposition into rabbit and incorporate a novel ocular component in the model. This PBPK model will help in preclinical to clinical translation of new therapies for ocular disorders and will help in the assessment of potential ocular toxicity for systemically administered antibody-based therapies.

Methods

Experimental Data.

We utilized data from several publications investigating the PK of full-size IgG antibodies in rabbits. All studies were carried in accordance with the Animal Welfare Act and were approved by the applicable Institutional Animal Care and Use Committee.

Data for the systemic PK of antibody comes from two studies in anthrax research. The first, is from a subset of data from Malkevich et al. [23]. In the relevant experiments, the authors dosed New Zealand White rabbits with Anthrivig (polyclonal human anthrax immunoglobulin, AIGIV), by intravenous infusion at 14.2 or 21.3 mg/kg bodyweight. Serial plasma samples were collected over 29 days and analyzed by ELISA[23]. In the second study, Nagy et al.[24]. investigators dosed New Zealand White rabbits with obiltoxaximab (chimeric monoclonal antibody) at 3, 10, or 30 mg/kg. Serum was collected over 28 days and analyzed by electrochemiluminescent assay[24].

Four additional sets of data contained intraocular PK of antibody after intravitreal administration in rabbits. The first, from Bakri et al.[25], provided the PK of bevacizumab (humanized antivascular endothelial growth factor, VEGF) in 20 Dutch-belted rabbits after intravitreal injection of 1.25 mg in one eye. On days 1, 3, 8, 15, and 29,terminal samples of serum, vitreous humor, and aqueous humor were collected [25]. The second data set comes from Nomoto et al.[26], who administered 1.25 mg bevacizumab intravitreally to a single eye in each of 24 Dutch-belted rabbits and collected plasma, retina, iris/ciliary body, vitreous humor, and aqueous humor at 1, 2, 4, and 12 weeks post-injection. In the third data set, Sinapis et al.[27] unilaterally injected 1.25 mg bevacizumab in 20 New Zealand White Rabbits and collected serum, vitreous humor, and aqueous humor on days 1, 2, 8, 15, and 29 after injection. The final data set comes from Gadkar et al. [28] (obtained from publication in Hutton-Smith et al.[5]) in which New Zealand White rabbits were administered one of several human antibodies or antibody fragments. The current study only utilizes the dataset for full-length IgG against glycoprotein D (α-gD). Rabbits received intravitreal injections of 0.5 mg/eye in both eyes. Terminal samples of serum, vitreous humor, aqueous humor, and retina were obtained at 0.25, 2, 8, 14, 21, and 28 days [28]. In all studies, antibody concentrations where determined by ELISA [26-28] or chemiluminescent immunoassay [25].

Platform PBPK Model.

The structure of the whole-body PBPK model, originally developed by Shah and Betts[16], is described in Figure 1. The model incorporates plasma and blood cell compartments, as well as 16 major tissues and an optional tumor compartment (not utilized in the present study). The 17th "other" compartment comprises all the remaining tissues not explicitly identified in the model. All tissues are connected by anatomical plasma/blood flow and lymphatic recirculation through the lymph nodes. Each of the 16 tissue compartments (except for the eye) is further sub-divided into the following 6 components: blood cells, plasma space, endosomal space, interstitial space, cell membrane, and cellular space (Figure 2)[16]. In this manner, we describe the flow of plasma (Q) into the tissue and the outward flow of plasma (Q-L) and lymph (L). IgG within the plasma space enters the tissue by two processes: (1) via paracellular pores using convective lymph flow, where the vascular reflection coefficient (σv) represents resistance to IgG convection by the vascular endothelial cells, or (2) via pinocytosis (CLup) into the endosomal space, where IgG may bind to FcRn and be recycled back into the plasma space (FR) or into the interstitial space (1-FR) via exocytosis. Unbound IgG in the endosomal space is degraded by a first-order process (Kdeg) in the lysosome. Once in the interstitial space, IgG is cleared by the flow of lymph where the interstitial reflection coefficient (σi) represents resistance to IgG convection by the lymphatic openings. Should the antibody in the interstitial space have a cellular target, it is tree to bind to antigen (Ag) expressed on the cell surface and be internalized (Kint_Ag-IgG). However, the antibodies selected as part of this study do not have targets expressed in rabbits. Therefore, parameters associated with antigen binding and internalization are set to zero.

The physiological parameters related to tissue volumes and fluid flows in the PBPK model were obtained from a variety of sources[29-32]. The values and descriptions for physiological parameters of the platform model are shown in Tables 1 and 2. The lymph flow for all tissues was set to 0.2% of plasma flow and the endosomal volume was set to 0.5% of the total tissue volume[33,15]. The fraction of IgG bound to FcRn that recycles back to the plasma space (FR) was set to 0.715[34]. The vascular reflection coefficients (σv) for each tissue were set *a priori* and are as follows: 0.85 for spleen, liver, and bone; 0.9 for kidney, thymus, small intestine, and pancreas; 0.95 for lung, heart, muscle, skin, adipose, large intestine, and other; and 0.99 for brain[35]. The interstitial reflection coefficient (σi) was set to 0.2 in all tissues[15]. The association (K_{on}) and dissociation (K_{off}) rates for human/humanized IgG binding to rabbit FcRn are $2.85x10^{7}$ $M^{-1}h^{-1}$ and 1.4 h^{-1}, respectively[36], Pinocytosis and exocytosis rate (CL_{up}), lysosomal degradation rate (K_{deg}), and FcRn concentration were set to 0.55 L/h, 32.2 h^{-1}, and $4.98x10^{-5}$ M, as reported previously [37,16], The proportionality constant (C_{LNLF}) between the rate at which IgG transfers into the plasma from the lymph node and the plasma flow itself was set to 9.1, as determined by Shah and Betts[16]. Equations for the platform PBPK model are provided below.

Blood Compartment

Plasma Space

$$\frac{d}{dt}C_{plasma} = (PLQ_{Heart} - LF_{Heart}) * C_{Heart_V} + (PLQ_{Kidney} - LF_{Kidney}) * C_{Kidney_V} + (PLQ_{Muscle} - LF_{Muscle}) * C_{Muscle_V} + (PLQ_{Skin} - LF_{Skin}) * C_{Skin_V} + (PLQ_{Brain} - LF_{Brain}) * C_{Brain_V} + (PLQ_{Adipose} - LF_{Adipose}) * C_{Adipose_V} + (PLQ_{Thymus} - LF_{Thymus}) * C_{Thymus_V} + ((PLQ_{Liver} - LF_{Liver}) + (PLQ_{S.Intestine} - LF_{S.Intestine}) + (PLQ_{L.Intestine} - LF_{L.Intestine}) + (PLQ_{Spleen} - LF_{Spleen}) + (PLQ_{Pancreas} - LF_{Pancreas})) * C_{Liver_V} + (PLQ_{Bone} - LF_{Bone}) * C_{Bone_V} + (PLQ_{Other} - LF_{Other}) * C_{Other_V} + 2\left((PLQ_{Eye} - LF_{Eye}) * f_{cho} * C_{Eye_V}\right) + 2\left((PLQ_{Eye} - LF_{Eye}) * f_{ret} * C_{Eye_V}\right) + 2\left((PLQ_{Eye} - LF_{Eye}) * (1 - f_{cho} - f_{ret}) * C_{Eye_V}\right) - (PLQ_{Lung} + LF_{Lung}) * C_{Plasma} + LF_{Lymph\,Node} * C_{Lymph\,Node_V} * \left(\frac{1}{V_{Plasma}}\right) \quad (1)$$

Blood Cell Space

$$\frac{d}{dt}C_{BC} = \left(BCQ_{Heart} * C_{Heart_{BC}} + BCQ_{Kidney}) * C_{Kidney_{BC}} + BCQ_{Muscle} * C_{Muscle_{BC}} + BCQ_{Skin} * C_{Skin_{BC}} + BCQ_{Brain} * C_{Brain_{BC}} + BCQ_{Adipose} * C_{Adipose_{BC}} + BCQ_{Thymus} * C_{Thymus_{BC}} + (BCQ_{Liver} + BCQ_{S.Intestine} + BCQ_{L.Intestine} + BCQ_{Spleen} + BCQ_{Pancreas}) * C_{Liver_{BC}} + BCQ_{Bone} * C_{Bone_{BC}} + BCQ_{Other} * C_{Other_{BC}} + 2(BCQ_{Eye} * f_{cho} * C_{Eye_{BC}}) + 2(BCQ_{Eye} * f_{ret} * C_{Eye_{BC}}) + 2(BCQ_{Eye} * (1 - f_{cho} - f_{ret}) * C_{Eye_{BC}}) - BCQ_{Lung} * C_{BC}\right) * \left(\frac{1}{V_{BC}}\right) \quad (2)$$

Lymph Node Compartment

$$\frac{d}{dt}C_{Lymph\ Node} = \Big((1 - ISRC_{Heart}) * LF_{Heart} * C_{Heart_I} + (1 - ISRC_{Kidney}) * LF_{Kidney} * C_{Kidney_I} + (1 - ISRC_{Muscle}) * LF_{Muscle} * C_{Muscle_I} + (1 - ISRC_{Skin}) * LF_{Skin} * C_{Skin} + (1 - ISRC_{Brain}) * LF_{Brain} * C_{Brain_I} + (1 - ISRC_{Adipose}) * LF_{Adipose} * C_{Adipose_I} + (1 - ISRC_{Thymus}) * LF_{Thymus} * C_{Thymus_I} + (1 - ISRC_{Liver}) * LF_{Liver} * C_{Liver_I} + (1 - ISRC_{S.Intestine}) * LF_{S.Intestine} * C_{S.Intestine_I} + (1 - ISRC_{L.Intestine}) * LF_{L.Intestine} * C_{L.Intestine_I} + (1 - ISRC_{Spleen}) * LF_{Spleen} * C_{Spleen_I} + (1 - ISRC_{Pancreas}) * LF_{Pancreas} * C_{Pancreas_I} + (1 - ISRC_{Bone}) * LF_{Bone} * C_{Bone_I} + (1 - ISRC_{Other}) * LF_{Other} * C_{Other_I} + 2(1 - ISRC_{Eye}) * LF_{Eye} * (1 - f_{Cho} - f_{Ret}) * C_{ICB_I} + 2(1 - ISRC_{Eye}) * LF_{Eye} * f_{Ret} * C_{Ret_I} + 2(1 - ISRC_{Eye}) * LF_{Eye} * f_{Cho} * C_{Cho_I} + (1 - ISRC_{Lung}) * LF_{Lung} * C_{Lung_I} - LF_{Lymph\ Node} * C_{Lymph\ Node}\Big) * \frac{1}{V_{Lymph\ Node}} \quad (3)$$

Typical Tissue Compartment

Vascular Space

$$\frac{d}{dt}C_{Tissue_V} = (PLQ_{Tissue} * C_{Lung_V} - (PLQ_{Tissue} - LF_{Tissue}) * C_{Tissue_V} - (1 - VRC_{Tissue}) * LF_{Tissue} * C_{Tissue_V} - CL_{up_{Tissue}} * C_{Tissue_V} + CL_{up_{Tissue}} * FR * C_{Tissue_{EB}}) * \frac{1}{V_{Tissue_V}} \quad (4)$$

Endosomal Space mAb unbound to FcRn

$$\frac{d}{dt}C_{Tissue_{EU}} = \frac{CL_{up_{Tissue}} * (C_{Tissue_V} + C_{Tissue_I})}{V_{Tissue_E}} - K_{on_{FcRn}} * C_{Tissue_{EU}} * (FcRn_{Tissue} + FcRn) + K_{off_{FcRn}} * C_{Tissue_{EB}} - K_{deg_{IgG}} * C_{Tissue_{EU}} \quad (5)$$

Endosomal Space mAb bound to FcRn

$$\frac{d}{dt}C_{Tissue_{EB}} = K_{on_{FcRn}} * C_{Tissue_{EU}} * (FcRn_{Tissue} + FcRn) - K_{off_{FcRn}} * C_{Tissue_{EB}} - \frac{CL_{up_{Tissue}} * C_{Tissue_{EB}}}{V_{Tissue_E}} \quad (6)$$

Endosomal space FcRn

$$\frac{d}{dt}FcRn_{Tissue} = K_{off_{FcRn}} * C_{Tissue_{EB}} - K_{on_{FcRn}} * C_{Tissue_{EU}} * (FcRn_{Tissue} + FcRn) + \frac{CL_{up_{Tissue}} * C_{Tissue_{EB}}}{V_{Tissue_E}} \quad (7)$$

Interstitial Space

$$\frac{d}{dt}C_{Tissue_I} = \left((1 - VRC_{Tissue}) * LF_{Tissue} * C_{Tissue_V} - (1 - ISRC_{Tissue}) * LF_{Tissue} * C_{Tissue_I} + CL_{up_{Tissue}} * (1 - FR) * C_{Tissue_{EB}} - CL_{up_{Tissue}} * C_{Tissue_I}\right) * \frac{1}{V_{Tissue_I}} \quad (8)$$

Blood Cell Space

$$\frac{d}{dt}C_{Tissue_{BC}} = \frac{BCQ_{Tissue} * (C_{Lung_{BC}} - C_{Tissue_{BC}})}{V_{Tissue_{BC}}} \quad (9)$$

Lung Compartment

Vascular Space

$$\frac{d}{dt}C_{Lung_V} = \left((PLQ_{Lung} + LF_{Lung}) * C_{Lung_V} - PLQ_{Lung} * C_{Lung_V} - (1 - VRC_{Lung}) * LF_{Lung} * C_{Lung_V} - CL_{up_{Lung}} * C_{Lung_V} + CL_{up_{Lung}} * FR * C_{Lung_{EB}}\right) * \frac{1}{V_{Lung_V}} \quad (10)$$

Liver Compartment

Vascular Space

$$\frac{d}{dt}C_{Liver_V} = (PLQ_{Liver} * C_{Lung_V} - (PLQ_{Liver} - LF_{Liver}) + (PLQ_{S.Intestine} - LF_{S.Intestine}) + (PLQ_{L.Intestine} - LF_{L.Intestine}) + (PLQ_{Spleen} - LF_{Spleen}) + (PLQ_{Pancreas} - LF_{Pancreas}) * C_{Liver_V} + (PLQ_{S.Intestine} - LF_{S.Intestine}) * C_{S.Intestine_V} + (PLQ_{L.Intestine} - LF_{L.Intestine}) * C_{L.Intestine_V} + (PLQ_{Spleen} - LF_{Spleen}) * C_{Spleen_V} + (PLQ_{Pancreas} - LF_{Pancreas}) * C_{Pancreas_V} - (1 - VRC_{Liver}) * LF_{Liver} * C_{Liver_V} - CL_{up_{Liver}} * C_{Liver_V} + CL_{up_{Liver}} * FR * C_{Liver_{EB}}) * \frac{1}{V_{Liver_V}} \quad (11)$$

Blood Cell Space

$$\frac{d}{dt}C_{Tissue_{BC}} = (BCQ_{Liver} * C_{Lung_{BC}} + BCQ_{S.Intestine} * C_{S.Intestine_{BC}} + BCQ_{L.Intestine} * C_{L.Intestine_{BC}} + BCQ_{Spleen} * C_{Spleen_{BC}} + BCQ_{Pancreas} * C_{Pancreas_{BC}} - (BCQ_{Liver} + BCQ_{S.Intestine} + BCQ_{L.Intestine} + BCQ_{Spleen} + BCQ_{Pancreas}) * C_{Liver_{BC}}) * \frac{1}{V_{Liver_{BC}}} \quad (12)$$

Lung and liver compartments not explicitly shown, share the same equations as a typical tissue.

Physiologically-Based Ocular Compartment.

As a novel expansion to the platform PBPK model, we have incorporated an anatomically and physiologically relevant ocular compartment. The overall structure of the new compartment is shown in Figure 3, and the physiologic parameters are provided in Tables 3, 4 and 5. The major tissues of the eye are represented, which include cornea, iris-ciliary body (ICB), aqueous humor (AH), lens, vitreous humor (VH), retina, and choroid. Plasma flow to the eye is fractionally divided into the ICB, choroid, and retina, and equal flow exits these tissues by both plasma and lymph flow.

Convection of fluid within the ocular humor compartments is also incorporated in the model. Aqueous humor produced by the ICB enters the aqueous chamber (QPtA) and exits via Schlemm's canal (QAH) or flows into the vitreous chamber (QBF). Fluid entering the vitreous chamber recirculates back into the aqueous chamber (QVA), undergoing anterior elimination, or undergoes bulk flow (QBF) to the retina and subsequently the choroid,

undergoing posterior elimination. Furthermore, the model allows for permeation of IgG at several major intraocular tissue interfaces.

As with the tissues in the platform PBPK model, the vascularized tissues of the eye are subdivided into smaller spaces (Figure 4), and the major mechanisms of antibody disposition described above are present. However, each intraocular tissue also contains components representing the unique fluid flows and interfaces found in the eye. As with the systemic reflection coefficients, reflection coefficients within the eye represent the level of resistance to IgG convection by the blood-aqueous barrier (σaq), the inner limiting membrane of the retina (σret), and the retinal pigment epithelium (σcho). These values are assumed to be high (i.e. 0.95, 0.99, and 0.99, respectively). Similar to the brain, the eye is known to be shielded from systemic circulation by the blood-aqueous barrier and the blood-retina barrier, thus the vascular reflection coefficient in the ocular tissues was set to 0.99 (the interstitial reflection coefficient remains 0.2). Equations for the ocular PBPK model are included below.

Cornea Compartment

$$\frac{d}{dt}C_{Cor} = (C_{Aq} - C_{Cor}) * PS_{Cor} \tag{13}$$

Aqueous Humor Compartment

$$\begin{aligned}\frac{d}{dt}C_{Aq} = (C_{Cor} - C_{Aq}) * PS_{Cor} + (C_{Lens} - C_{Aq}) * PS_{Lens} + \frac{C_{Vit} * Q_{VA}}{V_{Aq}} \\ + \frac{C_{ICB_V} * Q_{PtA} * (1 - RC_{Aq})}{V_{Aq}} \\ - \frac{C_{Aq} * (CL_{AH} + Q_{BF} + Q_{VA})}{V_{Aq}}\end{aligned} \tag{14}$$

Iris-Ciliary Body Compartment

Vascular Space

$$\begin{aligned}\frac{d}{dt}C_{ICB_V} = (PLQ_{Eye} * (1 - f_{cho} - f_{ret}) * C_{Lung_V} - (PLQ_{Eye} - LF_{Eye}) * \\ (1 - f_{cho} - f_{ret}) \\ * C_{ICB_V} - (1 - VRC_{Eye}) * LF_{Eye} * (1 - f_{cho} - f_{ret}) * \\ C_{ICB_V} - CL_{up_{ICB}} * C_{ICB_V} \\ * \frac{1}{V_{ICB_V}}\end{aligned} \tag{15}$$

Endosomal Space mAb unbound to FcRn

$$\frac{d}{dt}C_{ICB_{EU}} = \frac{CL_{up_{ICB}} * (C_{ICB_V} + C_{ICB_I})}{V_{ICB_E}} - K_{on_{FcRn}} * C_{ICB_{EU}} * (FcRn_{ICB} + FcRn) + K_{off_{FcRn}} * C_{ICB_{EB}} - K_{deg_{IgG}} * C_{ICB_{EU}} \quad (16)$$

Endosomal Space mAb bound to FcRn

$$\frac{d}{dt}C_{ICB_{EB}} = K_{on_{FcRn}} * C_{ICB_{EU}} * (FcRn_{ICB} + FcRn) - K_{off_{FcRn}} * C_{ICB_{EB}} - \frac{CL_{up_{ICB}} * C_{ICB_{EB}}}{V_{ICB_E}} \quad (17)$$

Endosomal Space FcRn

$$\frac{d}{dt}FcRn_{ICB} = K_{off_{FcRn}} * C_{ICB_{EB}} - K_{on_{FcRn}} * C_{ICB_{EU}} * (FcRn_{ICB} + FcRn) + \frac{CL_{up_{ICB}} * C_{ICB_{EB}}}{V_{ICB_E}} \quad (18)$$

Interstitial Space

$$\frac{d}{dt}C_{ICB_I} = \Big((1 - VRC_{Eye}) * LF_{Eye} * (1 - f_{Cho} - f_{Ret}) * C_{ICB_V} - (1 - ISRC_{Eye}) * LF_{Eye} * (1 - f_{Cho} - f_{Ret}) * C_{ICB_I} + CL_{Up_{ICB}} * (1 - FR) * C_{ICB_{EB}} - CL_{Up_{ICB}} * C_{ICB_I} + C_{Aq} * CL_{AH} - C_{ICB_I} * CL_{AH}\Big) * \frac{1}{V_{ICB_I}} \quad (19)$$

Blood Cell Space

$$\frac{d}{dt}C_{ICB_{BC}} = \frac{BCQ_{Eye} * (1 - f_{Cho} - f_{Ret}) * (C_{Lung_{BC}} - C_{ICB_{BC}})}{V_{ICB_{BC}}} \quad (20)$$

Lens Compartment

$$\frac{d}{dt}C_{Lens} = (C_{AQ} - C_{Lens}) * PS_{Lens} + (C_{Vit} - C_{Lens}) * PS_{Lens} \quad (21)$$

Vitreous Humor Compartment

$$\frac{d}{dt}C_{Vit} = (C_{Ret_I} - C_{Vit}) * PS_{Ret} + (C_{Lens} - C_{Vit}) * PS_{Lens} - \frac{C_{Vit} * Q_{VA}}{V_{Vit}} - \frac{C_{Vit} * Q_{BF} * (1 - RC_{Ret})}{V_{Vit}} + \frac{C_{Aq} * (Q_{BF} + Q_{VA})}{V_{vit}} \quad (22)$$

Retina Compartment

Vascular Space

$$\frac{d}{dt}C_{Ret_V} = (PLQ_{Eye} * f_{Ret} * C_{Lung_V} - (PLQ_{Eye} - LF_{Eye}) * f_{Ret} * C_{Ret_V} - (1 - VRC_{Eye}) * LF_{Eye} * f_{Ret} * C_{Ret_V} - CL_{up_{Ret}} * C_{Ret_V} + CL_{up_{Ret}} * FR * C_{Ret_{EB}}) * \frac{1}{V_{Ret_V}} \quad (23)$$

Endosomal Space mAb unbound to FcRn

$$\frac{d}{dt}C_{Ret_{EU}} = \frac{CL_{up_{Ret}} * (C_{Ret_V} + C_{Ret_I})}{V_{Ret_E}} - K_{on_{FcRn}} * C_{Ret_{EU}} * (FcRn_{Ret} + FcRn) + K_{off_{FcRn}} * C_{Ret_{EB}} - K_{deg_{IgG}} * C_{Ret_{EU}} \quad (24)$$

Endosomal Space mAb bound to FcRn

$$\frac{d}{dt}C_{Ret_{EB}} = K_{on_{FcRn}} * C_{Ret_{EU}} * (FcRn_{Ret} + FcRn) - K_{off_{FcRn}} * C_{Ret_{EB}} - \frac{CL_{up_{Ret}} * C_{Ret_{EB}}}{V_{Ret_E}} \quad (25)$$

Endosomal Space FcRn

$$\frac{d}{dt}FcRn_{Ret} = K_{off_{FcRn}} * C_{Ret_{EB}} - K_{on_{FcRn}} * C_{Ret_{EU}} * (FcRn_{Ret} + FcRn) + \frac{CL_{up_{Ret}} * C_{Ret_{EB}}}{V_{Ret_E}} \quad (26)$$

Interstitial Space

$$\frac{d}{dt}C_{Ret_I} = \Big((1 - VRC_{Eye}) * LF_{Eye} * f_{Ret} * C_{Ret_V} - (1 - ISRC_{Eye}) * LF_{Eye} * f_{Ret} * C_{Ret_I} + CL_{UpRet} * (1 - FR) * C_{Ret_{EB}} - CL_{UpRet} * C_{Ret_I}\Big) * \frac{1}{V_{Ret_I}} + (C_{Vit} - C_{Ret_I}) * PS_{Ret} + (C_{Cho_I} - C_{Ret_I}) * PS_{Cho} + \frac{C_{Vit} * Q_{BF} * (1 - RC_{Ret})}{V_{Ret_I}} - \frac{C_{Ret_I} * Q_{BF} * (1 - RC_{Cho})}{V_{Ret_I}} \quad (27)$$

Blood Cell Space

$$\frac{d}{dt}C_{Ret_{BC}} = \frac{BCQ_{Eye} * f_{Ret} * (C_{Lung_{BC}} - C_{Ret_{BC}})}{V_{Ret_{BC}}} \quad (28)$$

Choroid Compartment

Vascular Space

$$\frac{d}{dt}C_{Cho_V} = (PLQ_{Eye} * f_{Cho} * C_{Lung_V} - (PLQ_{Eye} - LF_{Eye}) * f_{Cho} * C_{Cho_V} - (1 - VRC_{Eye}) * LF_{Eye} * f_{Cho} * C_{Cho_V} - CL_{up_{Cho}} * C_{Cho_V} + CL_{up_{Cho}} * FR * C_{Cho_{EB}} + C_{Cho_I} * Q_{BF}) * \frac{1}{V_{Cho_V}} \quad (29)$$

Endosomal Space mAb unbound to FcRn

$$\frac{d}{dt}C_{Cho_{EU}} = \frac{CL_{up_{Cho}} * (C_{Cho_V} + C_{Cho_I})}{V_{Cho_E}} - K_{on_{FcRn}} * C_{Cho_{EU}} * (FcRn_{Cho} + FcRn) + K_{off_{FcRn}} * C_{Cho_{EB}} - K_{deg_{IgG}} * C_{Cho_{EU}} \quad (30)$$

Endosomal Space mAb bound to FcRn

$$\frac{d}{dt}C_{Cho_{EB}} = K_{on_{FcRn}} * C_{Cho_{EU}} * (FcRn_{Cho} + FcRn) - K_{off_{FcRn}} * C_{Cho_{EB}} - \frac{CL_{up_{Cho}} * C_{Cho_{EB}}}{V_{Cho_E}} \quad (31)$$

Endosomal Space FcRn

$$\frac{d}{dt}FcRn_{Cho} = K_{off_{FcRn}} * C_{Cho_{EB}} - K_{on_{FcRn}} * C_{Cho_{EU}} * (FcRn_{Cho} + FcRn) + \frac{CL_{up_{Cho}} * C_{Cho_{EB}}}{V_{Cho_E}} \quad (32)$$

Interstitial Space

$$\frac{d}{dt}C_{Cho_I} = \left((1 - VRC_{Eye}) * LF_{Eye} * f_{Cho} * C_{Cho_V} - (1 - ISRC_{Eye}) * LF_{Eye} * f_{Cho} * C_{Cho_I} + CL_{Up_{Cho}} * (1 - FR) * C_{Cho_{EB}} - CL_{Up_{Cho}} * C_{Cho_I}\right) * \frac{1}{V_{Cho_I}} + (C_{Ret_I} - C_{Cho_I}) * PS_{Cho} + \frac{C_{Ret_I} * Q_{BF} * (1 - RC_{Cho})}{V_{Cho_I}} - \frac{C_{Cho_I} * Q_{BF}}{V_{Cho_I}} \quad (33)$$

Blood Cell Space

$$\frac{d}{dt}C_{Cho_{BC}} = \frac{BCQ_{Eye} * f_{cho} * (C_{Lung_{BC}} - C_{Cho_{BC}})}{V_{Cho_{BC}}} \quad (34)$$

PBPK Model Estimation and Simulation.

Model fitting was carried out in ADAPT 5 [38] with the intravitreal dose parameter being estimated. Data from collected tissues were fit simultaneously to estimate the dose in each study utilizing intravitreal dosing. Model simulations were carried out in Berkeley Madonna (version 8.3.23.0) software[39]. All values for parameters in the PBPK model are ascertained from previously published literature sources and the intravitreal dose amount estimated using ADAPT 5. Initially, performance of the platform PBPK model was evaluated by simulation of plasma PK of exogenous antibody after intravenous administration. After addition of the novel ocular component, the model was validated by estimation of PK in the serum, aqueous humor, vitreous humor, and retina after intravitreal administration of antibody. Predictive capability of the model was assessed quantitatively by calculation of symmetric mean absolute percentage error (SMAPE) (Equation 1) between the AUC of the simulated PK profile (AUC_{sim}) and the average AUC of the observed PK profiles for indicated niAbs (AUC_{obs}). Using this method, a 2-fold overprediction or a 2-fold under-prediction would give an SMAPE of 33%.

$$SMAPE = \frac{|AUC_{sim} - AUC_{obs}|}{\frac{1}{2}(|AUC_{sim}| + |AUC_{obs}|)} * 100\% \quad (35)$$

Results

In general, all plasma and tissue PK datasets in rabbit were well characterized by the PBPK model. The simulated AUC of the concentration vs time curve was within 2-fold of the average observed AUC in almost all cases as determined by SMAPE.

Dose Estimation with the PBPK Model.

As outlined in the “Experimental Data” section above, three of the four studies administered bevacizumab to one eye at a dose of 1.25 mg. However, the PK profiles for each study showed variability in the observed concentration vs. time course. Moreover, in the Sinapis et al. [27] study, serum was collected by allowing blood to clot at room temperature for 1 hr before centrifugation rather than immediate centrifugation, potentially resulting in bevacizumab loss and low observed serum concentrations of the antibody. Therefore, serum data was not used when estimating the dose parameter for the Sinapis et al. [27] dataset. The dose parameters for each intravitreal dose study was estimated with confidence and are shown in Table 6.

Performance of the Platform PBPK Model.

Figure 5 shows the simulated and observed concentration vs. time profile of AIGIV and obiltoxaximab after an intravenous infusion. Both the simulated and observed data are dose normalized. In general, the simulation captures the observed profiles, with some discrepancy at earlier time points, but minimal deviation from most of the data. The average SMAPE of the prediction was 5.34%. The excellent performance of the model validates the successful translation of the platform model to rabbits.

Performance of the Ocular PBPK Model.

Figure 6 shows the simulated and observed concentration vs. time profiles of all α-gD and bevacizumab data sets after intravitreal injection. In plasma, the slow appearance of antibody is recapitulated, although the terminal phase shows large variability between the two molecules. Furthermore, rapid appearance of antibody in the aqueous humor, iris/ciliary body, and retina are simulated in accordance with observed effects. Lastly, pharmacokinetics in the vitreous humor are simulated appropriately with the terminal decline parallel in all the ocular tissues. The SMAPE of the predictions in in all ocular tissues are in Table 6. Despite slight variation in the PK of α-gD and the three bevacizumab data sets, the model performs very well showing no systematic over- or under-prediction.

Discussion

PBPK models are an important tool in translating preclinical pharmacology of antibodies to the clinic. An important objective of PBPK modelling is to characterize the system with physiologically relevant parameters so that the plasma and tissue PK of a drug can be accurately characterized simply with the knowledge of drug specific parameters obtained *in vitro* (e.g. affinity with FcRn). While PBPK models of antibody disposition have been well established in many species, such as mice, rats, monkeys, and human, to date, there is no validated PBPK model for antibody disposition in rabbits. In this manuscript, we sought to

develop a PBPK model for rabbit because is a widely used species, particularly in development of antibody therapeutics for ocular disorders.

The platform PBPK model proposed by Shah and Betts[16] and presented in Figures 1 and 2 provides a basis for developing PBPK models for new species, as we have done here with rabbits. As an important validation step, the rabbit PBPK model accurately simulates the time course of antibody concentration in plasma after intravenous dosing with minimal predictive error (Figure 5). A key attribute of these simulations is that all parameters, both related to the system and to the drug, were fixed *a priori*. However, rabbits are rarely used with the intention of measuring whole body tissue pharmacokinetics. Therefore, tissue-level data for antibody PK is not readily available, with reported studies having few collection times or unclear dosing regimens, which is unsuitable to use for our modeling endeavors[40,41]. Nevertheless, reliable data in rabbit is available from the literature regarding ocular disposition of antibodies.

Rabbits are the most common species used in assessing ocular pharmacokinetics and toxicity[18,17]. Thus, a rabbit PBPK model including a detailed eye component would be a valuable tool in ocular drug development. As a frequently used species, the ocular anatomy and physiology of the rabbit is well known and has been incorporated into the PBPK model. While maintaining the whole-body and drug parameters, the ocular model accurately simulates the pharmacokinetics of IgG in both the serum and several individual ocular tissues: aqueous humor, iris/ciliary body, vitreous humor, and retina (figure 6). Such prediction across tissues is extremely advantageous in ocular research where some individual tissues, such as retina or iris-ciliary body, are difficult to isolate and analyze. For example, taps of the aqueous and/or vitreous chamber (i.e. direct sampling) can be used for data collection in a single animal over time, and the concentration in the hard-to-reach tissues can then be simulated using the ocular PBPK model. This predictive capability is of even greater importance in the clinical setting, where aqueous taps are the only samples typically available.

While our proposed model focuses on full-length IgG therapies (150 kDa), smaller molecular weight biologics are of more interest for treating ocular disease. Indeed, all FDA-approved macromolecules for ocular disorders have molecular weights below 150 kDa: aflibercept (115 kDa), pegaptanib (50 kDa), ranibizumab (48 kDa), ocriplasmin (27.2 kDa), and brolucizumab (26 kDa). The current iteration of the platform PBPK model is unsuited to model smaller biologics as it assumes a single pore exists in the vascular endothelium through which a therapeutic antibody enters tissues. For lower molecular weight protein therapeutics, a model incorporating the “two pore hypotheses” of extravasation would be more appropriate[42,43]. Recently, our lab has applied the “two pore hypothesis” to the platform PBPK model[37]. The next step is to integrate the “two pore hypotheses” with the ocular PBPK model to predict the PK of smaller compounds after intravitreal administration.

Although ocular therapy currently centers on lower molecular weight protein therapeutics, modelling full-length IgG exposure in the eye is critical in assessing ocular toxicities. Targeted cancer therapies carry a risk of toxicity in healthy tissues that express the target antigen even at low levels. In phase I and phase II trials of the anti-HER2 ADC trastuzumab

emtansine, between 31.3 and 46.4% of patients had ocular adverse events[44,45]. For ipilimumab, Maker et al. [46] observed severe ocular toxicities in 35% of patients treated with the anti-CTLA-4 antibody. For cetuximab, the anti-EGFR antibody has been associated with several ocular adverse events including dry eye, blepharitis, and trichomegaly[47,48]. Our ocular PBPK model has the potential to predict drug concentrations in various tissues of the eye after systemic administration, and, when combined with knowledge of antigen expression, it provides a tool to assess potential risk of ocular toxicity.

Conclusions

In summary, we have presented a new platform PBPK model for antibody disposition in rabbits. Additionally, we have incorporated a novel physiologically relevant ocular compartment to the whole-body model, which incorporates the unique anatomy of the eye. Our ocular PBPK model successfully predicts the PK of an exogenous antibody in the plasma and the ocular tissues after intravitreal administration. Prediction of ocular PK with our model will aid in the preclinical to clinical translation of novel ocular therapeutics, and assessment of potential drug-induced ocular toxicities. In the future, the capabilities of the ocular PBPK model can be expanded by incorporating the “two pore hypothesis” to accurately predict the PK of smaller molecular weight protein therapeutics.

Acknowledgements

D.K.S is supported by NIH grants GM114179, AI138195, and R01CA246785.

References

1. The Global Economic Cost of Visual Impairment (2010). Access Economics,
2. Wong WL, Su X, Li X, Cheung CM, Klein R, Cheng CY, Wong TY (2014) Global prevalence of age-related macular degeneration and disease burden projection for 2020 and 2040: a systematic review and meta-analysis. Lancet Glob Health 2 (2):e106–116. doi:10.1016/S2214-109X(13)70145-1 [PubMed: 25104651]
3. Global $10.4 Bn Wet Age-Related Macular Degeneration Market to 2024 - Rising Prevalence of AMD, Lack of a Specific Treatment, and Increasing Aging Population (2019). GlobeNewswire, 2019/5/15/,
4. Hutton-Smith LA, Gaffney EA, Byrne HM, Maini PK, Schwab D, Mazer NA (2016) A Mechanistic Model of the Intravitreal Pharmacokinetics of Large Molecules and the Pharmacodynamic Suppression of Ocular Vascular Endothelial Growth Factor Levels by Ranibizumab in Patients with Neovascular Age-Related Macular Degeneration. Mol Pharm 13 (9):2941–2950. doi:10.1021/acs.molpharmaceut.5b00849 [PubMed: 26726925]
5. Hutton-Smith LA, Gaffney EA, Byrne HM, Maini PK, Gadkar K, Mazer NA (2017) Ocular Pharmacokinetics of Therapeutic Antibodies Given by Intravitreal Injection: Estimation of Retinal Permeabilities Using a 3-Compartment Semi-Mechanistic Model. Mol Pharm 14 (8):2690–2696. doi:10.1021/acs.molpharmaceut.7b00164 [PubMed: 28631484]
6. Park SJ, Choi Y, Na YM, Hong HK, Park JY, Park KH, Chung JY, Woo SJ (2016) Intraocular Pharmacokinetics of Intravitreal Aflibercept (Eylea) in a Rabbit Model. Invest Ophthalmol Vis Sci 57 (6):2612–2617. doi:10.1167/iovs.16-19204 [PubMed: 27258433]
7. Mordenti J, Cuthbertson RA, Ferrara N, Thomsen K, Berleau L, Licko V, Allen PC, Valverde CR, Meng YG, Fei DT, Fourre KM, Ryan AM (1999) Comparisons of the intraocular tissue distribution, pharmacokinetics, and safety of 125I-labeled full-length and Fab antibodies in rhesus monkeys following intravitreal administration. Toxicol Pathol 27 (5):536–544. doi:10.1177/019262339902700507 [PubMed: 10528633]

8. Kheir WJ, Sniegowski MC, El-Sawy T, Li A, Esmaeli B (2014) Ophthalmic complications of targeted cancer therapy and recently recognized ophthalmic complications of traditional chemotherapy. Surv Ophthalmol 59 (5):493–502. doi:10.1016/j.survophthal.2014.02.004 [PubMed: 25130892]

9. Renouf DJ, Velazquez-Martin JP, Simpson R, Siu LL, Bedard PL (2012) Ocular toxicity of targeted therapies. J Clin Oncol 30 (26):3277–3286. doi:10.1200/JCO.2011.41.5851 [PubMed: 22649132]

10. Hager T, Seitz B (2013) Ocular side effects of biological agents in oncology: what should the clinician be aware of? Onco Targets Ther 7:69–77. doi:10.2147/OTT.S54606 [PubMed: 24391443]

11. Eaton JS, Miller PE, Mannis MJ, Murphy CJ (2015) Ocular Adverse Events Associated with Antibody-Drug Conjugates in Human Clinical Trials. J Ocul Pharmacol Ther 31 (10):589–604. doi:10.1089/jop.2015.0064 [PubMed: 26539624]

12. Covell DG, Barbet J, Holton OD, Black CD, Parker RJ, Weinstein JN (1986) Pharmacokinetics of monoclonal immunoglobulin G1, F(ab')2, and Fab' in mice. Cancer Res 46 (8):3969–3978 [PubMed: 3731067]

13. Baxter LT, Zhu H, Mackensen DG, Jain RK (1994) Physiologically based pharmacokinetic model for specific and nonspecific monoclonal antibodies and fragments in normal tissues and human tumor xenografts in nude mice. Cancer Res 54 (6):1517–1528 [PubMed: 8137258]

14. Ferl GZ, Wu AM, DiStefano JJ 3rd (2005) A predictive model of therapeutic monoclonal antibody dynamics and regulation by the neonatal Fc receptor (FcRn). Ann Biomed Eng 33 (11):1640–1652. doi:10.1007/s10439-005-7410-3 [PubMed: 16341929]

15. Garg A, Balthasar JP (2007) Physiologically-based pharmacokinetic (PBPK) model to predict IgG tissue kinetics in wild-type and FcRn-knockout mice. J Pharmacokinet Pharmacodyn 34 (5):687–709. doi:10.1007/s10928-007-9065-1 [PubMed: 17636457]

16. Shah DK, Betts AM (2012) Towards a platform PBPK model to characterize the plasma and tissue disposition of monoclonal antibodies in preclinical species and human. J Pharmacokinet Pharmacodyn 39 (1):67–86. doi:10.1007/s10928-011-9232-2 [PubMed: 22143261]

17. del Amo EM, Urtti A (2015) Rabbit as an animal model for intravitreal pharmacokinetics: Clinical predictability and quality of the published data. Exp Eye Res 137:111–124. doi:10.1016/j.exer.2015.05.003 [PubMed: 25975234]

18. Short BG (2008) Safety evaluation of ocular drug delivery formulations: techniques and practical considerations. Toxicol Pathol 36 (1):49–62. doi:10.1177/0192623307310955 [PubMed: 18337221]

19. Pepin-Covatta S, Lutsch C, Grandgeorge M, Lang J, Scherrmann JM (1996) Immunoreactivity and pharmacokinetics of horse anti-scorpion venom F(ab')2-scorpion venom interactions. Toxicol Appl Pharmacol 141 (1):272–277. doi:10.1006/taap.1996.0284 [PubMed: 8917700]

20. Riviere G, Choumet V, Audebert F, Sabouraud A, Debray M, Scherrmann JM, Bon C (1997) Effect of antivenom on venom pharmacokinetics in experimentally envenomed rabbits: toward an optimization of antivenom therapy. J Pharmacol Exp Ther 281 (1):1–8 [PubMed: 9103473]

21. Ismail M, Abd-Elsalam MA, Al-Ahaidib MS (1998) Pharmacokinetics of 125I-labelled Walterinnesia aegyptia venom and its distribution of the venom and its toxin versus slow absorption and distribution of IGG, F(AB')2 and F(AB) of the antivenin. Toxicon 36 (1):93–114. doi:10.1016/s0041-0101(97)00062-7 [PubMed: 9604285]

22. Gutierrez JM, Leon G, Lomonte B (2003) Pharmacokinetic-pharmacodynamic relationships of immunoglobulin therapy for envenomation. Clin Pharmacokinet 42 (8):721–741. doi:10.2165/00003088-200342080-00002 [PubMed: 12846594]

23. Malkevich NV, Basu S, Rudge TL Jr., , Clement KH, Chakrabarti AC, Aimes RT, Nabors GS, Skiadopoulos MH, Ionin B (2013) Effect of anthrax immune globulin on response to BioThrax (anthrax vaccine adsorbed) in New Zealand white rabbits. Antimicrob Agents Chemother 57 (11):5693–5696. doi:10.1128/AAC.00460-13 [PubMed: 23979740]

24. Nagy CF, Mondick J, Serbina N, Casey LS, Carpenter SE, French J, Guttendorf R (2017) Animal-to-Human Dose Translation of Obiltoxaximab for Treatment of Inhalational Anthrax Under the US FDA Animal Rule. Clin Transl Sci 10 (1):12–19. doi:10.1111/cts.12433 [PubMed: 27925405]

25. Bakri SJ, Snyder MR, Reid JM, Pulido JS, Singh RJ (2007) Pharmacokinetics of intravitreal bevacizumab (Avastin). Ophthalmology 114 (5):855–859. doi:10.1016/j.ophtha.2007.01.017 [PubMed: 17467524]
26. Nomoto H, Shiraga F, Kuno N, Kimura E, Fujii S, Shinomiya K, Nugent AK, Hirooka K, Baba T (2009) Pharmacokinetics of bevacizumab after topical, subconjunctival, and intravitreal administration in rabbits. Invest Ophthalmol Vis Sci 50 (10):4807–4813. doi:10.1167/iovs.08-3148 [PubMed: 19324856]
27. Sinapis CI, Routsias JG, Sinapis AI, Sinapis DI, Agrogiannis GD, Pantopoulou A, Theocharis SE, Baltatzis S, Patsouris E, Perrea D (2011) Pharmacokinetics of intravitreal bevacizumab (Avastin(R)) in rabbits. Clin Ophthalmol 5:697–704. doi:10.2147/OPTH.S19555 [PubMed: 21629577]
28. Gadkar K, Pastuskovas CV, Le Couter JE, Elliott JM, Zhang J, Lee CV, Sanowar S, Fuh G, Kim HS, Lombana TN, Spiess C, Nakamura M, Hass P, Shatz W, Meng YG, Scheer JM (2015) Design and Pharmacokinetic Characterization of Novel Antibody Formats for Ocular Therapeutics. Invest Ophthalmol Vis Sci 56 (9):5390–5400. doi:10.1167/iovs.15-17108 [PubMed: 26275136]
29. Johnson RL, Gilbert M, Meschia G, Battaglia FC (1985) Cardiac output distribution and uteroplacental blood flow in the pregnant rabbit: a comparative study. Am J Obstet Gynecol 151 (5):682–686. doi:10.1016/0002-9378(85)90165-6 [PubMed: 3976768]
30. Davies B, Morris T (1993) Physiological parameters in laboratory animals and humans. Pharm Res 10 (7):1093–1095. doi:10.1023/a:1018943613122 [PubMed: 8378254]
31. Gerlowski LE, Jain RK (1983) Physiologically based pharmacokinetic modeling: principles and applications. J Pharm Sci 72 (10):1103–1127. doi:10.1002/jps.2600721003 [PubMed: 6358460]
32. Sweeney LM, Kirman CR, Gannon SA, Thrall KD, Gargas ML, Kinzell JH (2009) Development of a physiologically based pharmacokinetic (PBPK) model for methyl iodide in rats, rabbits, and humans. Inhal Toxicol 21 (6):552–582. doi:10.1080/08958370802601569 [PubMed: 19519155]
33. Swartz MA (2001) The physiology of the lymphatic system. Adv Drug Deliv Rev 50 (1-2):3–20 [PubMed: 11489331]
34. Urva SR, Yang VC, Balthasar JP (2010) Physiologically based pharmacokinetic model for T84.66: a monoclonal anti-CEA antibody. J Pharm Sci 99 (3):1582–1600. doi:10.1002/jps.21918 [PubMed: 19774657]
35. Sarin H (2010) Physiologic upper limits of pore size of different blood capillary types and another perspective on the dual pore theory of microvascular permeability. J Angiogenes Res 2:14. doi:10.1186/2040-2384-2-14 [PubMed: 20701757]
36. Szikora B, Hiripi L, Bender B, Kacskovics I, Ilias A (2017) Characterization of the interactions of rabbit neonatal Fc receptor (FcRn) with rabbit and human IgG isotypes. PLoS One 12 (9):e0185662. doi:10.1371/journal.pone.0185662 [PubMed: 28957416]
37. Li Z, Shah DK (2019) Two-pore physiologically based pharmacokinetic model with de novo derived parameters for predicting plasma PK of different size protein therapeutics. J Pharmacokinet Pharmacodyn 46 (3):305–318. doi:10.1007/s10928-019-09639-2 [PubMed: 31028591]
38. D'Argenio DZ, Schumitzky A, Wang X (2009) ADAPT 5 User's Guide: Pharmacokinetic/ Pharmacodynamic Systems Analysis Software. Biomedical Simiulations Resource, Los Angeles
39. Macey R, Oster G, Zahnley T (2009) Berkeley Madonna User's Guide.
40. Chakrabarti M, Cheng KT, Spicer KM, Kirsch WM, Fowler SD, Kelln W, Griende S, Nehlsen-Cannarella S, Willerson R, Spicer SS, et al. (1995) Biodistribution and radioimmunopharmacokinetics of 131I-Ama monoclonal antibody in atherosclerotic rabbits. Nucl Med Biol 22 (6):693–697. doi:10.1016/0969-8051(95)00008-l [PubMed: 8535329]
41. Lin YS, Nguyen C, Mendoza JL, Escandon E, Fei D, Meng YG, Modi NB (1999) Preclinical pharmacokinetics, interspecies scaling, and tissue distribution of a humanized monoclonal antibody against vascular endothelial growth factor. J Pharmacol Exp Ther 288 (1):371–378 [PubMed: 9862791]
42. Rippe B, Haraldsson B (1987) Fluid and protein fluxes across small and large pores in the microvasculature. Application of two-pore equations. Acta Physiol Scand 131 (3):411–428. doi:10.1111/j.1748-1716.1987.tb08257.x [PubMed: 3321914]

43. Rippe B, Haraldsson B (1994) Transport of macromolecules across microvascular walls: the two-pore theory. Physiol Rev 74 (1):163–219. doi:10.1152/physrev.1994.74.1.163 [PubMed: 8295933]
44. Beeram M, Krop IE, Burris HA, Girish SR, Yu W, Lu MW, Holden SN, Modi S (2012) A phase 1 study of weekly dosing of trastuzumab emtansine (T-DM1) in patients with advanced human epidermal growth factor 2-positive breast cancer. Cancer 118 (23):5733–5740. doi:10.1002/cncr.27622 [PubMed: 22648179]
45. Burris HA 3rd, , Rugo HS, Vukelja SJ, Vogel CL, Borson RA, Limentani S, Tan-Chiu E, Krop IE, Michaelson RA, Girish S, Amler L, Zheng M, Chu YW, Klencke B, O'Shaughnessy JA (2011) Phase II study of the antibody drug conjugate trastuzumab-DM1 for the treatment of human epidermal growth factor receptor 2 (HER2)-positive breast cancer after prior HER2-directed therapy. J Clin Oncol 29 (4):398–405. doi:10.1200/JCO.2010.29.5865 [PubMed: 21172893]
46. Maker AV, Yang JC, Sherry RM, Topalian SL, Kammula US, Royal RE, Hughes M, Yellin MJ, Haworth LR, Levy C, Allen T, Mavroukakis SA, Attia P, Rosenberg SA (2006) Intrapatient dose escalation of anti-CTLA-4 antibody in patients with metastatic melanoma. J Immunother 29 (4):455–463. doi:10.1097/01.cji.0000208259.73167.58 [PubMed: 16799341]
47. Borkar DS, Lacouture ME, Basti S (2013) Spectrum of ocular toxicities from epidermal growth factor receptor inhibitors and their intermediate-term follow-up: a five-year review. Support Care Cancer 21 (4):1167–1174. doi:10.1007/s00520-012-1645-y [PubMed: 23151647]
48. Fraunfelder FT, Fraunfelder FW (2012) Trichomegaly and other external eye side effects associated with epidermal growth factor. Cutan Ocul Toxicol 31 (3):195–197. doi:10.3109/15569527.2011.636118 [PubMed: 22122121]
49. Struble C, Howard S, Relph J (2014) Comparison of ocular tissue weights (volumes) and tissue collection techniques in commonly used preclinical animal species. Acta Ophthalmologica 92 (s253):0–0. doi:10.1111/j.1755-3768.2014.S005.x
50. del Amo EM, Rimpelä A-K, Heikkinen E, Kari OK, Ramsay E, Lajunen T, Schmitt M, Pelkonen L, Bhattacharya M, Richardson D, Subrizi A, Turunen T, Reinisalo M, Itkonen J, Toropainen E, Casteleijn M, Kidron H, Antopolsky M, Vellonen K-S, Ruponen M, Urtti A (2017) Pharmacokinetic aspects of retinal drug delivery. Progress in Retinal and Eye Research 57:134–185. doi:10.1016/j.preteyeres.2016.12.001 [PubMed: 28028001]
51. Nilsson SFE, Alm A (2012) Determination of Ocular Blood Flows with the Microsphere Method In: Schmetterer L, Kiel J (eds) Ocular Blood Flow. Springer Berlin Heidelberg, Berlin, Heidelberg, pp 25–47. doi:10.1007/978-3-540-69469-4_2
52. Fatt I, Hedbys BO (1970) Flow of water in the sclera. Exp Eye Res 10 (2):243–249. doi:10.1016/s0014-4835(70)80035-5 [PubMed: 5484767]
53. Maurice DM (1987) Flow of water between aqueous and vitreous compartments in the rabbit eye. Am J Physiol 252 (1 Pt 2):F104–108. doi:10.1152/ajprenal.1987.252.1.F104 [PubMed: 3812693]
54. Prausnitz MR, Noonan JS (1998) Permeability of cornea, sclera, and conjunctiva: a literature analysis for drug delivery to the eye. J Pharm Sci 87 (12):1479–1488 [PubMed: 10189253]
55. Wang Q, Chan S, Yang JY, You B, Wang YX, Jonas JB, Wei WB (2016) Vascular Density in Retina and Choriocapillaris as Measured by Optical Coherence Tomography Angiography. Am J Ophthalmol 168:95–109. doi:10.1016/j.ajo.2016.05.005 [PubMed: 27183862]
56. Ames A 3rd, , Nesbett FB (1966) Intracellular and extracellular compartments of mammalian central nervous tissue. J Physiol 184 (1):215–238. doi:10.1113/jphysiol.1966.sp007912 [PubMed: 5921539]
57. Wang JC, Lains I, Providencia J, Armstrong GW, Santos AR, Gil P, Gil J, Talcott KE, Marques JH, Figueira J, Vavvas DG, Kim IK, Miller JW, Husain D, Silva R, Miller JB (2017) Diabetic Choroidopathy: Choroidal Vascular Density and Volume in Diabetic Retinopathy With Swept-Source Optical Coherence Tomography. Am J Ophthalmol 184:75–83. doi:10.1016/j.ajo.2017.09.030 [PubMed: 28988899]
58. Mac Gabhann F, Demetriades AM, Deering T, Packer JD, Shah SM, Duh E, Campochiaro PA, Popel AS (2007) Protein transport to choroid and retina following periocular injection: theoretical and experimental study. Ann Biomed Eng 35 (4):615–630. doi:10.1007/s10439-006-9238-x [PubMed: 17277991]

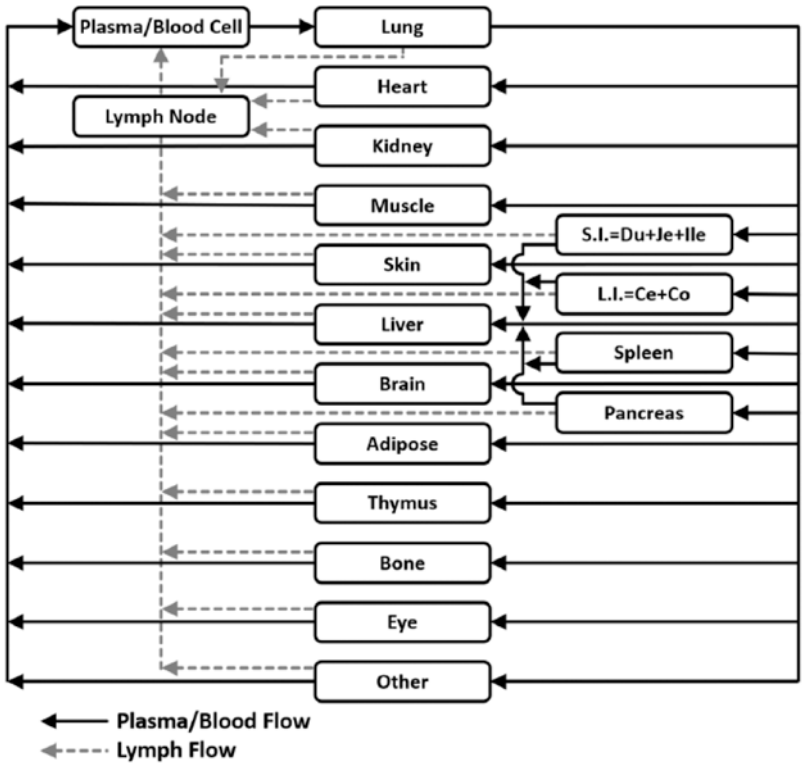

Fig. 1.

Schematic of the whole body PBPK model for antibody distribution. Rectangular compartments represent organs and solid and dashed arrows represent blood and lymph flow, respectively. Each tissue contains several sub-compartments as shown in Figure 2.

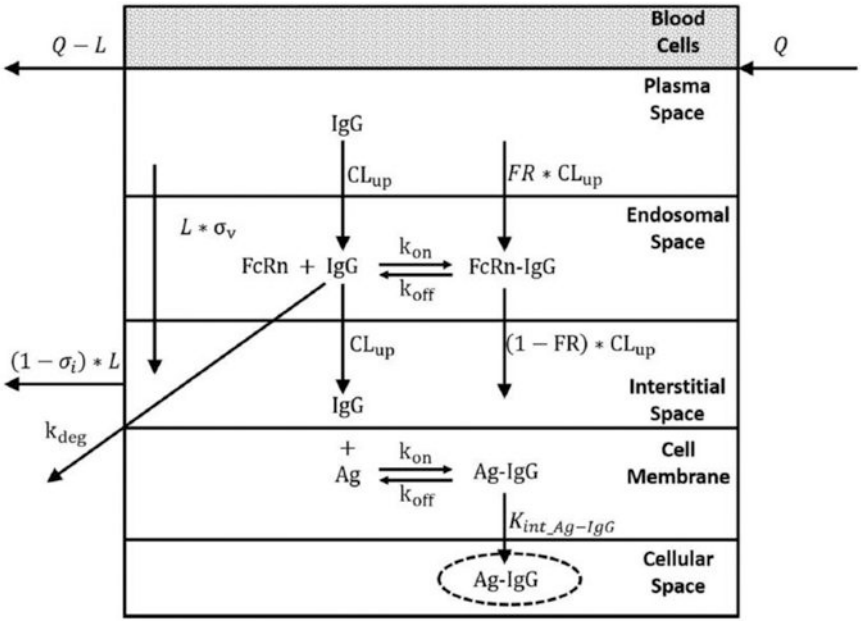

Fig. 2.

Schematic of tissue-level structure of the PBPK model. Please refer to the text for description of the processes involved in antibody disposition.

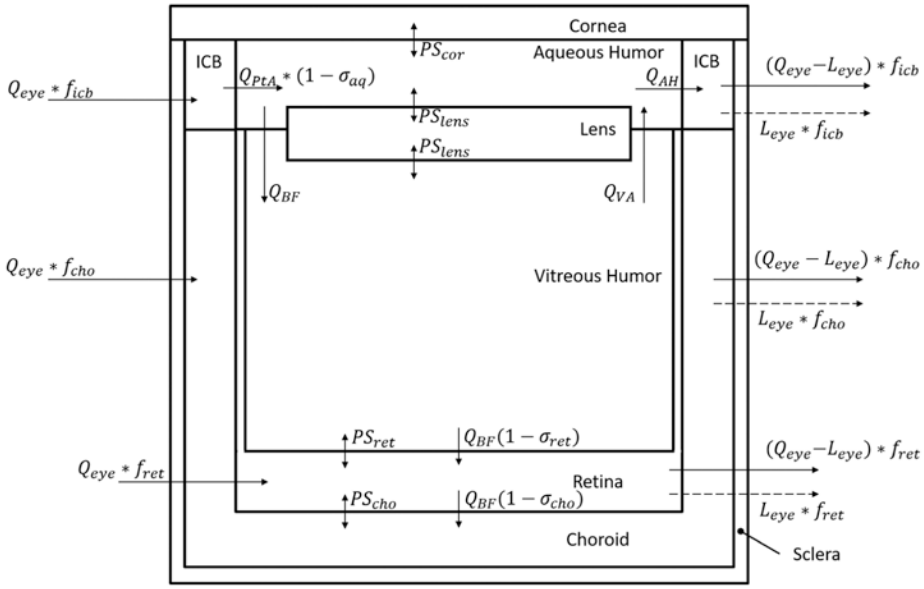

Fig. 3.

Structural schematic of the physiologically-based ocular compartment. The compartments are connected in an anatomical manner including blood, lymph, and intraocular fluid flows, and accounts for permeation at interfaces between tissues. The vascularized tissues are further divided in sub compartments as shown in Figure 5.

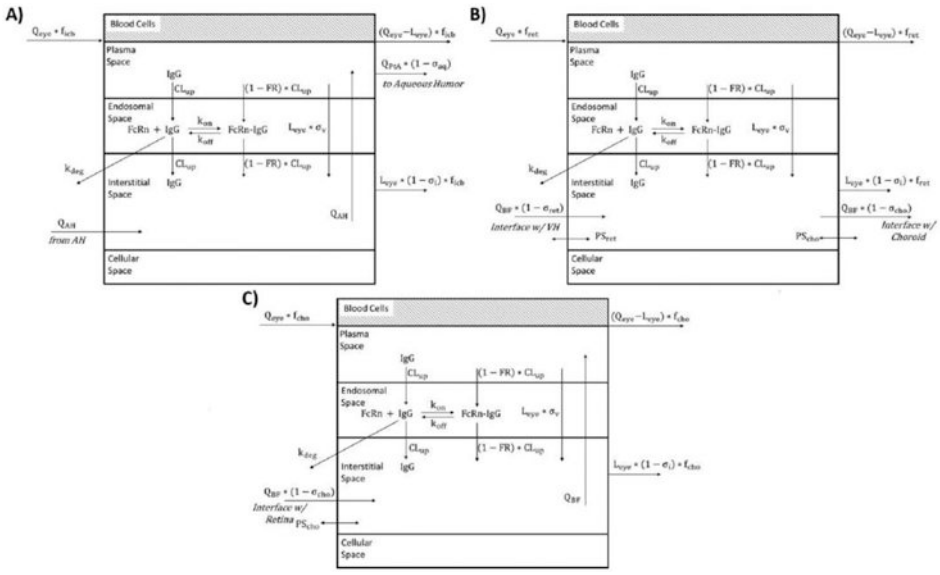

Fig. 4.

Schematic of tissue-level model for vascularized tissues in the ocular compartment, including (A) Iris-Ciliary Body, (B) Retina, and (C) Choroid.

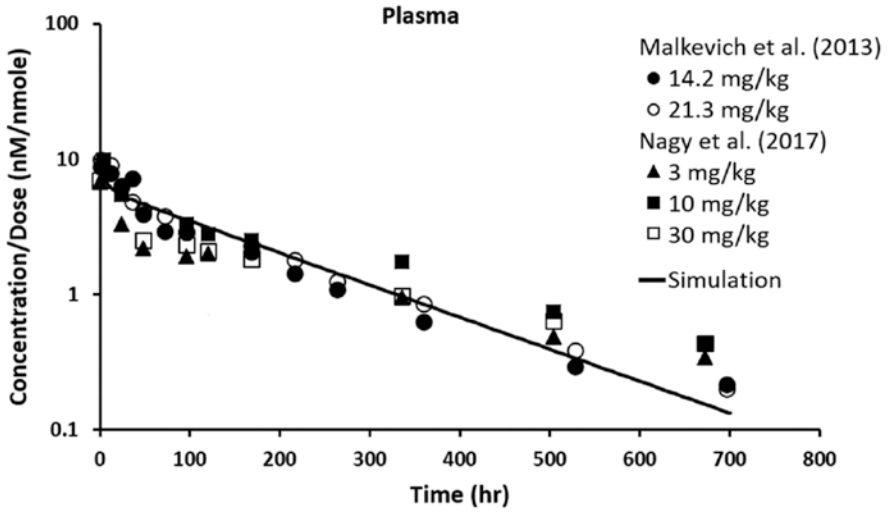

Fig. 5.

Observed (icons) and simulated (line) pharmacokinetics of intravenously-dosed monoclonal antibodies in rabbits. Data and simulation are dose normalized.

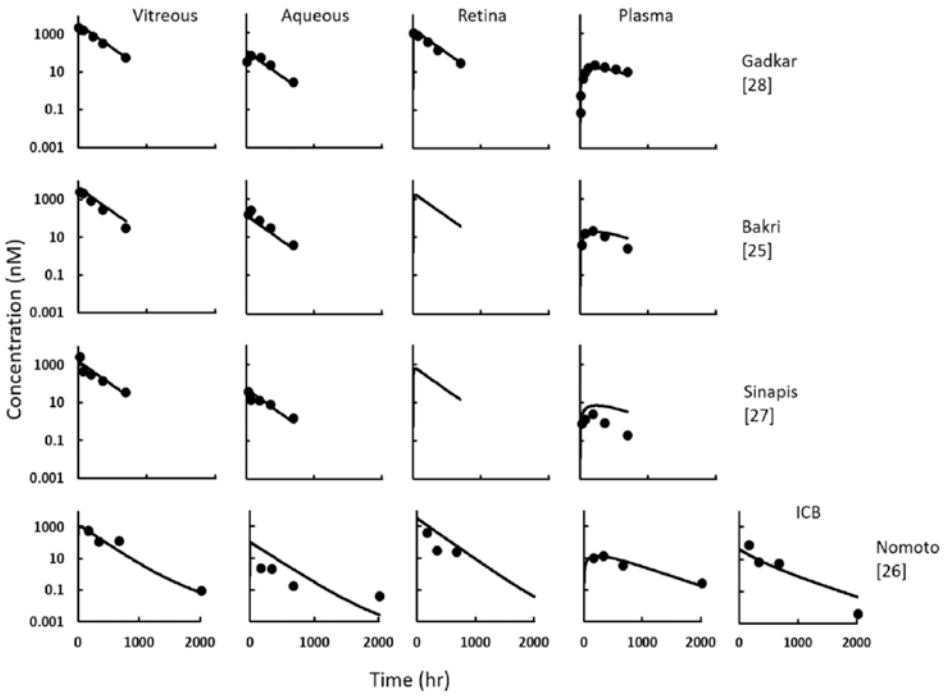

Fig. 6.

Observed (circles) and simulated (line) pharmacokinetics of intravitreally-dosed monoclonal antibodies that are non-targeting in rabbits.

Table 1.

Physiological model parameters for rabbit.

	Total Volume (L)	Plasma Volume (L)	Blood Cell Volume (L)	Interstitial Volume (L)	Endosomal Volume (L)	Cellular Volume (L)	Plasma Flow (L/h)	Blood Cell Flow (L/h)
Lung	0.0170	0.00247	0.00123	0.00320	0.0000850	0.0100	21.2	10.6
Heart	0.00600	0.000231	0.000116	0.000600	0.0000300	0.00502	0.768	0.384
Kidney	0.0150	0.00158	0.000788	0.00300	0.0000750	0.0103	3.69	1.85
Muscle	1.35	0.0351	0.0176	0.162	0.00675	1.13	6.21	3.11
Skin	0.110	0.00209	0.00105	0.0332	0.000550	0.0711	1.63	0.813
Brain	0.0140	0.000518	0.000259	5.60E-06	0.0000700	0.0134	0.380	0.190
Adipose	0.120	0.00120	0.000600	0.0162	0.000600	0.10128	1.28	0.641
Thymus S.	0.00410	0.000228	0.000114	0.000697	2.05E-05	0.00374	0.0224	0.0112
Intestine L.	0.0600	0.00144	0.000720	0.00564	0.000300	0.0524	2.21	1.10
Intestine	0.0300	0.000720	0.000360	0.00282	0.000150	0.0262	0.564	0.282
Spleen	0.00100	0.000282	0.000141	0.000150	0.00000500	0.000583	0.360	0.180
Pancreas	0.00360	0.000648	0.000324	0.000432	0.0000180	0.00263	0.144	0.0720
Liver	0.100	0.0115	0.00575	0.0163	0.000500	0.0690	0.163	0.0815
Bone	0.310	0.0127	0.00636	0.0310	0.00155	0.264	1.86	0.930
Ly. Node	0.0103	--	--	--	--	0.0103	--	--
Other	0.2493	0.0103	0.00517	0.0422	0.00123	0.230	1.89	0.943
Plasma	0.110	--	--	--	--	--	21.2	--
Blood Cells	0.055	--	--	--	--	--	--	10.6

Table 2.

Glossary of parameters used in the PBPK model

Parameter	Units	Definition
PLQ_i	L/h	Plasma flow to the tissue "i"
BCQ_i	L/h	Blood cell flow to the tissue "i"
L_i	L/h	Lymph flow from the tissue "i"
V_{Plasma}, V_{BC}, $V_{LymphNode}$	L	Volumes of the central plasma, central blood cell, and lymph node compartments
$V_i^V, V_i^{BC}, V_i^E, V_i^{IS}, V_i^C$	L	Volumes of the vascular, blood cell, endosomal, interstitial, and cellular compartments for the tissue "i"
C_{Plasma}, C_{BC}, $C_{LymphNode}$	nM	Concentrations in the central plasma, central blood cell, and lymph node compartments
$C_i^V, C_i^{BC}, C_i^{EUnbound}, C_i^{EBound}, C_i^{IS}, C_i^{CBound}$	nM	Concentrations in the vascular, blood cell, endosomal (Unbound and Bound), interstitial, and cellular (Bound) compartments for the tissue "i"
$FcRn$	M	Concentration of FcRn in the endosomal space
$\sigma_i^V, \sigma_i^{IS}$	–	Vascular and lymph reflection coefficients
$K_{on}^{FcRn}, K_{on}^{Ag}$	$1/M/h$	Association rate constants between mAb and FcRn and mAb and Antigen
$K_{off}^{FcRn}, K_{off}^{Ag}$	$1/h$	Dissociation rate constants between mAb and FcRn and mAb and Antigen
FR	–	Fraction of FcRn bound mAb that recycles to the vascular space
CL_{up}	$L/h/L$	Rate of pinocytosis and exocytosis per unit endosomal space of the vascular endothelium
K_{deg}	$1/h$	First-order degradation rate constant of FcRn-unbound mAb in the endosomal space

Table 3.

Physiological parameters for the ocular component of the rabbit PBPK model.

Parameter	Value	Source
V_{Cornea} (mL)	0.0887	[49]
V_{AH} (mL)	0.306	Struble et al. [49]
V_{VH} (mL)	1.41	[49]
Q_{eye} (L/h)	0.0483	[50]
L_{eye} (L/h)	Q_eye*0.002	Calculated
f_{icb}	0.131	[51]
f_{ret}	0.00911	[51]
f_{cho}	0.860	[51]
Q_{BF} (L/h)	0.00003	[52]
Q_{VA} (L/h)	0.000008	[53]
Q_{PtA} (L/h)	$Q_{AH} - Q_{VA} + Q_{BF}$	Calculated
Q_{AH} (L/h)	0.000212	[50]
σ_{ret}	0.95	Fixed
σ_{cho}	0.99	Fixed
σ_{aq}	0.99	Fixed
PS_{cor} (L/h)	1.19×10^{-8}	[54]
PS_{lens} (L/h)	0	Fixed
PS_{ret} (L/h)	2.64×10^{-6}	[5]
PS_{cho} (L/h)	2.88×10^{-6}	[5]

Table 4.

Physiological parameters for tissue sub-compartments in the ocular model.

		Fraction of Total Volume comprising				
	Total Volume (μL)	**Plasma Volume**	**Blood Cell Volume**	**Interstitial Volume**	**Endosomal Volume**	**Cellular Volume**
Retina	42.0	0.287[55]	0.1435	0.32[56]	0.005	0.245
Choroid	28.4	0.23[57]	0.115	0.4[58]	0.005	0.25
ICB[a]	87.8	0.23	0.115	0.4	0.005	0.25

[a]ICB was assumed to have the same composition as choroid due to structural similarity

Table 5.

Glossary of parameters used in the ocular compartment of the PBPK model.

Parameter	Units	Definition
V_{Cornea}, V_{AH}, V_{VH}	*L*	Volumes of the cornea, aqueous humor, and vitreous humor compartments
Q_{eye}	*L /h*	Blood flow to the eye
L_{eye}	*L /h*	Lymph flow from the eye
f_{icb}, f_{ret}, f_{cho}	–	Fraction of total blood and total lymph flow entering and exiting the iris-ciliary body, retina, and choroid
Q_{BF}	*L /h*	Bulk flow of fluid from the anterior eye to the posterior eye
Q_{VA}	*L /h*	Flow of fluid from vitreous chamber to aqueous chamber
Q_{PtA}	*L /h*	Flow of fluid from plasma to aqueous humor (i.e. rate of aqueous humor production)
Q_{AH}	*L /h*	Flow of fluid from aqueous humor returning to plasma (i.e. rate of aqueous humor drainage)
σ_{ret}, σ_{cho}	–	Bulk flow reflection coefficients in the retina and choroid
σ_{aq}	–	Plasma-to-aqueous humor reflection coefficient
PS_{cor}, PS_{lens}, PS_{ret}, PS_{cho}	*L/h*	Permeability Surface Area products for mAb in cornea, lens, retina, and choroid

Table 6.

Estimated dose amount administered in intravitreal dosing studies and SMAPE of the PBPK model in prediction of AUC in ocular tissues.

			SMAPE				
Estimated Dose (mg)	**CV%**	**Study**	**Vitreous Humor**	**Aqueous Humor**	**Retina**	**Plasma**	**Iris/Ciliary Body**
0.754	8.03	Gadkar[28]	11.0	4.19	9.43	19.3	
0.926	14.1	Bakri[25]	23.4	30.5		23.4	
0.696	2.39	Sinapis[27]	15.4	14.7		72.7	
0.343	15.6	Nomoto[26]	5.09	89.6	11.2	12.5	15.1